STP 1631, 2020 / available online at www.astm.org / doi: 10.1520/STP163120190128

Christof Torrent,[1] André Bauer,[1] Malte Vollmer,[1]
and Thomas Niendorf[1]

On the Challenges toward Realization of Functionally Graded Structures by Electron Beam Melting—Fe-Base Shape Memory Alloy and Stainless Steel

Citation

C. Torrent, A. Bauer, M. Vollmer, and T. Niendorf, "On the Challenges toward Realization of Functionally Graded Structures by Electron Beam Melting—Fe-Base Shape Memory Alloy and Stainless Steel," in *Structural Integrity of Additive Manufactured Materials and Parts*, ed. N. Shamsaei and M. Seifi (West Conshohocken, PA: ASTM International, 2020), 20–33. http://doi.org/10.1520/STP163120190128[2]

ABSTRACT

In the present study, an iron-manganese-aluminum-nickel (Fe-Mn-Al-Ni) shape memory alloy was processed on an austenitic steel (AISI 304) build platform by electron beam melting in order to study the feasibility of realizing functionally graded structures consisting of two different materials (i.e., a functional and a structural material). Compression specimens consisting of the processed shape memory alloy and the austenitic build platform in equal parts were investigated. The microstructure was analyzed in the as-built state and after different heat treatments, focusing on the interface between both materials. Scanning electron microscopy and electron backscatter diffraction measurements were conducted to reveal the relation between processing steps and the microstructural evolution. It is shown that the microstructure after the electron beam melting process is characterized by a preferred ⟨001⟩ orientation with respect to the build direction and that a suitable microstructure for good pseudoelastic

Manuscript received October 30, 2019; accepted for publication February 25, 2020.
[1]Universität Kassel, Institute of Materials Engineering, Mönchebergstraße 3, 34125 Kassel, Germany
C. T. https://orcid.org/0000-0002-9487-0853, A. B. https://orcid.org/0000-0002-9392-803X,
M. V. https://orcid.org/0000-0002-8098-8498, T. N. https://orcid.org/0000-0003-2622-5817
[2]Fourth ASTM Symposium on *Structural Integrity of Additive Manufactured Materials and Parts* on October 7–10, 2019 in National Harbor, MD, USA.

performance can be realized by post-processing heat treatments. Finally, incremental strain tests up to 12% compressive strain were conducted to analyze the overall mechanical performance of the specimens.

Keywords
additive manufacturing, shape memory alloy, austenitic steel, functionalized structures, secondary recrystallization

Introduction

Apart from the unprecedented design freedom, additive manufacturing (AM) provides the possibility of influencing the microstructure of specimens and components as well as pathways toward processing and obtaining new materials. As an example, silver–iron compounds and other nanoparticle modified materials, which usually do not form an alloy in common melting processes, can be processed by AM.[1,2] Moreover, it is shown that materials with tailored microstructural and mechanical properties over arbitrary component directions can be obtained by using different parameters during processing.[3,4] Thus, it is possible to build a specimen and simultaneously tailor its microstructure. An advanced approach is the combined processing of different materials (e.g., by applying powder layers of various materials). In this study, it is demonstrated that specimens consisting of two different materials, that is, a functional shape memory alloy (SMA) and a structural material, can be realized by AM.

The specimens in the electron beam melting (EBM) process are built layer-by-layer from material powder. The first layer is built up directly on the platform used. This is followed by moving the platform downward, spreading new powder and selective melting. Eventually, the parts grow along the build axis. In most cases, the platform and the specimen consist of different materials, and the interface between both is characterized by diffusion and compositional changes.[5] Moreover, the thermal conditions change during the process and are influenced by preheating, melting, and spreading new powder. This thermal history is often referred to as in situ annealing and intrinsic heat treatment, respectively.[6] While the influence of the thermal history cannot be completely suppressed, the influence of diffusion and compositional changes in vicinity of the platform is usually minimized by cutting the specimens well above the affected zone between specimens and platform. Therefore, the behavior in the specimen–platform interface has been barely investigated so far. However, for multi-material AM, the interface between the different materials is of high interest. In the present study, the platform is used as a part of the specimens in order to gain insights into the microstructural evolution of the interface and the mechanical behavior of specimens consisting of two different materials (i.e., an iron-base SMA and an austenitic steel).

Due to their characteristic thermoelastic martensitic transformation, SMAs are a promising class of materials exhibiting functional properties such as pseudoelasticity, one-way effect, and two-way effect.[7] These effects can be used for actuation,

damping, and sensing applications, respectively. In recent years, processing of SMAs by AM attracted a lot of attention.[8–10] Unique microstructural features upon AM (e.g., induced by directional solidification) can be beneficial for the functional performance of SMAs.[11] One of the alloy systems of particular interest is the recently developed iron-manganese-aluminum-nickel (Fe-Mn-Al-Ni) alloy. It shows a low Clausius-Clapeyron slope of 0.53 MPa/K and a wide temperature range for pseudoelastic application (−196°C to 240°C).[12] Good pseudoelastic properties have been observed in single[13–18] as well as in oligocrystalline[12,19–24] states. However, the material is characterized by a highly anisotropic behavior leading to constraints, most importantly resulting in severe stress concentrations at grain boundary triple junctions. Therefore, it is of crucial importance to obtain highly textured microstructures through processing. Moreover, it was shown that oligocrystalline structures consisting of grains exceeding the cross section of the specimens improve the pseudoelastic behavior in this SMA (referred to as *bamboo structures*). Recently, a cyclic heat treatment procedure was developed for a copper (Cu)-based SMA leading to oligocrystalline and single crystalline structures in the order of several centimeters.[25] The same kind of procedure was successfully applied to Fe-Mn-Al-Ni.[23,26]

In 2015, Niendorf et al.[8] demonstrated the feasibility of processing Fe-Mn-Al-Ni by AM, i.e., by selective laser melting (SLM). Good pseudoelastic properties in compression were revealed. However, the high cooling rates as well as the evolution of residual stresses, both being characteristic for SLM, were shown to lead to process-induced cracking preferentially along grain boundaries.[23] To account for these shortcomings, EBM was used in the present study in order to minimize crack formation. EBM is a hot powder bed process (i.e., being conducted at elevated process temperatures and lower cooling rates), eventually leading to decreasing residual stresses and the formation of the ductile γ phase at the grain boundaries.[23] Advantages of using Fe-Mn-Al-Ni as the SMA in focus are the expected good compatibility to AISI 304 and the relatively low dependency of the functional properties on the chemical composition as compared to other SMAs, such as nickel-titanium (Ni-Ti). To evaluate the microstructure within the additively manufactured SMA as well as in the diffusion zone between the SMA and the austenitic steel, different characterization methods were used, i.e., optical microscopy (OM), scanning electron microscopy (SEM), electron backscatter diffraction (EBSD), and energy dispersive X-ray spectroscopy (EDS). Moreover, different post-processing heat treatments were conducted to obtain a coarse-grained microstructure, which is crucial for a good pseudoelastic performance. Afterward, the mechanical behavior was investigated by incremental strain tests (ISTs) accompanied by in situ OM in order to correlate the overall performance with local microstructural features.

Materials and Experimental Methods

Fe-36Mn-8Al-8.5Ni (wt%) with a powder size ranging from 60 µm to 100 µm was processed using an Arcam A2X EBM (Arcam, Mölndal, Sweden) machine on an

TABLE 1 Parameter sets employed for processing of specimens and relative density measured by contrast image analysis based on OM micrographs

Set	Current (mA)	Voltage (kV)	Power (W)	Speed (mm/s)	Hatch (mm)	Layer (mm)	Volume Energy (J/mm^3)	Rel. Density (%)
#1	3	60	180	3,000	0.05	0.05	24	92.1
#2	3.5	60	210	3,000	0.05	0.05	28	98.4
#3	4	60	240	3,000	0.05	0.05	32	98.5

AISI 304 stainless steel platform. Three parameter sets, differing in terms of volume energy, were used (table 1). Preheating to 950°C was conducted for all conditions. Compression specimens with dimensions of 3 by 3 by 6 mm^3 were wire-cut by electrical discharge machining in a way that the loading direction was parallel to the build direction (BD). Care was taken to ensure that the interface between AISI 304 and Fe-Mn-Al-Ni was roughly in the middle of the specimens. For further investigations, selected specimens of each parameter set were subjected to subsequent thermal treatments, that is, solution annealing at 1,225°C for 1 h followed by water quenching in 80°C warm water and alternatively a cyclic heat treatment according to the procedure shown in figure 1 in order to promote abnormal grain growth (AGG). The cyclic heat treatment consists of four cycles between 1,225°C and 900°C with dwell times of 30 min and 15 min, respectively, and four cycles between 1,150°C and 900°C with dwell times of 15 min each. The heating and cooling rates

FIG. 1 Cyclic heat treatment procedure used in this study to promote abnormal grain growth in the Fe-Mn-Al-Ni SMA.

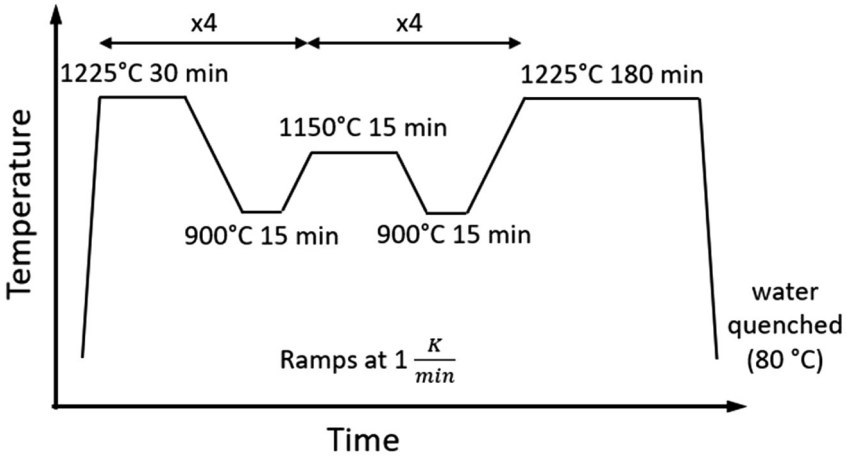

were 1 K min^{-1}. Afterward, the specimens were solution annealed at 1,225°C for 3 h and finally quenched in 80°C warm water. As it was shown by Omori et al.,[25] the driving force for AGG is provided by subgrain structures introduced during formation and dissolution of a second phase. In further studies, it was demonstrated that the misorientation of the subgrain structures and, thus, the driving force for AGG, increased when cycles with upper temperatures only slightly above the solvus temperature were used.[27,28] For further details on the cyclic heat treatment procedure, readers are referred to a recent study by Vollmer et al.[28] Finally, specimens were immediately aged for 3 h at 200°C in order to form β precipitates, which are essential for the thermoelastic martensitic transformation in the Fe-Mn-Al-Ni SMA,[17] and to avoid any room-temperature aging effects.[15,21]

Microstructure analysis was carried out on planes parallel to the build direction in order to investigate the interface between the materials as well as the porosity distribution over the build height. For that purpose, specimens were ground to 5 μm grit size and vibropolished to 0.02 μm using colloidal suspension. Microstructural characterization was conducted using OM as well as an SEM system operated at a nominal voltage of 20 kV. The relative density of the specimens was evaluated by pore analysis based on OM images. Polished surfaces with an area of about 1.5 by 1.5 mm^2 were analyzed in as-built condition using the software ImageJ. The SEM system was equipped with EBSD and EDS units for grain orientation analysis and determination of the chemical composition, respectively. Compression tests on a cyclic heat-treated Fe-Mn-Al-Ni/AISI 304 specimen as well as on an AISI 304 reference specimen subjected to the same heat treatment were performed using a servohydraulic testing machine operated in displacement control at a rate of 5 μm s^{-1}. Strain was measured by an extensometer having a gauge length of 12 mm being directly attached to the compression grips, which were considered to be absolutely rigid. Strain values were recalculated according to the actual size of the specimens. Incremental strain tests up to 12% strain with a step size of 1% were performed. For in situ characterization, a Keyence microscope with a VH Z100 objective was mounted directly in front of the servohydraulic testing machine. Surface images in the loaded conditions as well as in the unloaded conditions of each increment were recorded.

Results and Discussion

MICROSTRUCTURAL CHARACTERIZATION OF THE AS-BUILT STATE

In order to study the impact of the applied volume energy, three different beam currents were used. The micrographs (OM) in **figure 2** show characteristic microstructures of the different sets of specimens in the as-built state. Obviously, Specimen #1 is characterized by a large number of pores. This can be related to the low volume energy and lack of fusion defects, respectively.[29] In contrast, Specimens #2 and #3 show nearly the same relative density of about 98.5% (**table 1**). At higher volume energy densities, a tendency toward columnar solidification of the α phase can

FIG. 2 Optical micrographs of the additively manufactured Fe-Mn-Al-Ni in as-built state (build directions are highlighted by white arrows). Conditions shown differ by the used volume energy: (*A*) 24 J/mm^3; (*B*) 28 J/mm^3; and (*C*) 32 J/mm^3.

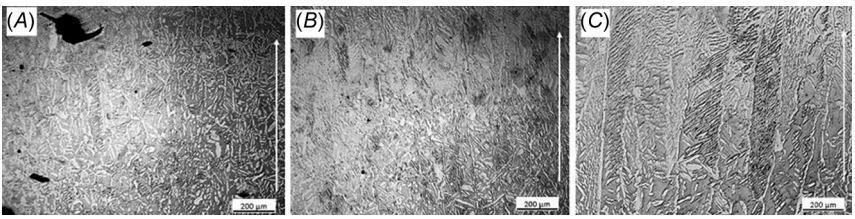

be seen. In line with the results and conclusions detailed in Kurz, Bezençon, and Gäumann,[30] it is very likely that lower solidification and cooling rates as well as changes in the melt pool shape and depths caused by the higher beam currents and energy density, respectively, are responsible for the columnar solidification in these specimens. Eventually, microstructure evolution can be rationalized by the strong relationships between the solidification and cooling rate, the thermal gradient, and the resulting grain morphology.[30]

In all three conditions, a large fraction of serrated γ-phase is formed, being sufficient to effectively suppress the formation of cracks alongside the grain boundaries during cooling.[23] The high-volume fraction of γ phase can be related to the high temperature prevailing within the chamber during processing. However, since the γ phase is detrimental to the pseudoelastic behavior,[31] additional heat treatments are necessary in order to obtain adequate functional properties.

The AISI 304/Fe-Mn-Al-Ni interfaces of the as-built conditions are shown in **figure 3**. In all conditions, small pores are visible directly at the interface (dashed arrows in **fig. 3*C***) as well as a segregated, dark spotted area with a thickness of about 30 to 50 µm next to the interface (dashed circles in **fig. 3**). Unfortunately, resolution of the EDS system is not high enough to analyze the composition of these spots. In contrast to the microstructure shown in **figure 2**, the ductile γ phase can hardly be observed in the diffusion zone near the interface between the SMA and the platform. Changes in local chemical composition are, thus, assumed to be the reason for the occurrence of individual transcrystalline cracks in the vicinity of the interface as marked by the dashed arrows in **figure 3*B***. It is very likely that the lack of ductile γ-phase is linked to chromium diffusion from the AISI 304 to the Fe-Mn-Al-Ni, as it is well known that chromium stabilizes the α phase in Fe-Mn-Al-Ni.[28] Moreover, a loss of the γ-stabilizing manganese was observed for each parameter set in comparison to the original powder composition as is highlighted in **figure 4**. Manganese is known to stabilize the γ phase; however, the element is also known to evaporate due to its very low vapor pressure in EBM processing; still, the loss of

FIG. 3 Backscattered electron (BSE) micrographs showing the interface area of Fe-Mn-Al-Ni and AISI 304 built with different volume energies: (*A*) 24 J/mm^3; (*B*) 28 J/mm^3; and (*C*) 32 J/mm^3. Porosity along the interface is highlighted (dashed arrows in *C*) as well as transcrystalline cracks (dashed arrows in *B*); furthermore, a dark spotted area can be seen within the first 50 µm of every build job (white ovals). In each condition, a white solid arrow highlights the BD.

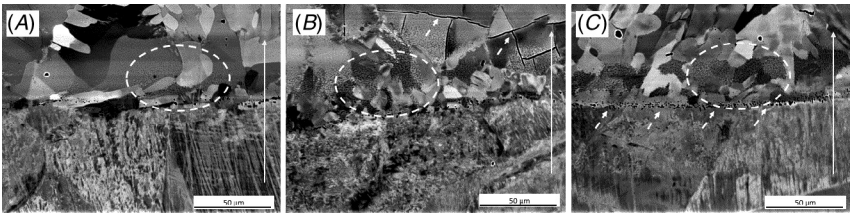

FIG. 4 Chemical analysis of the as-received powder and the material processed by the three investigated parameter sets as obtained by EDS analysis.

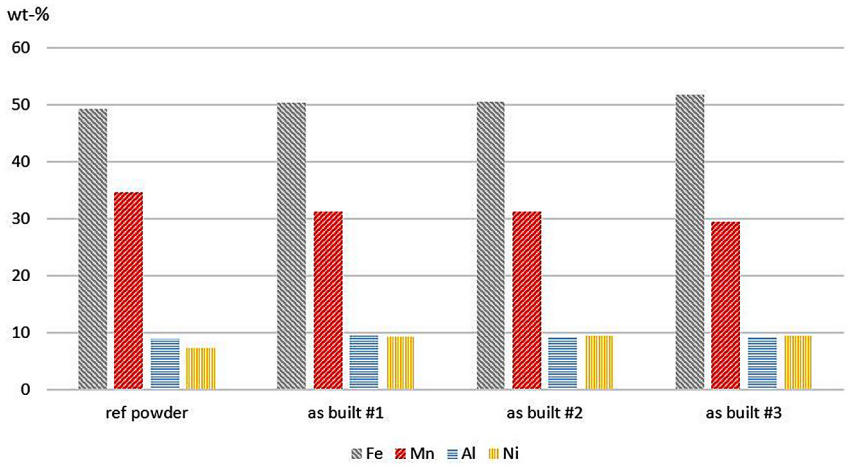

manganese can be controlled by the energy density applied for melting as has been shown very recently for a medium-manganese steel.[32]

MICROSTRUCTURAL CHARACTERIZATION AFTER DIFFERENT HEAT TREATMENTS

Microstructures present in the vicinity of the interface of the SMA and the austenitic steel after solution annealing are shown in figure 5. It should be emphasized that AGG occurred randomly in the specimens, independent from the volume energy

FIG. 5 BSE micrographs of the interface after solution annealing at 1,225°C for 1 h. Grain coarsening can be clearly seen in (*A*) and hardly in (*B*) (24 J/mm^3 and 28 J/mm^3). In both conditions, the microstructure differs in direct vicinity of the build plate. There is no coarsening; however, differing microstructure up to about 1 mm from the build plate can be seen in (*C*) (32 J/mm^3; see white marker). The dark segregations in direct vicinity of the interface have become larger in comparison to the as-built state. BD is highlighted by white arrows.

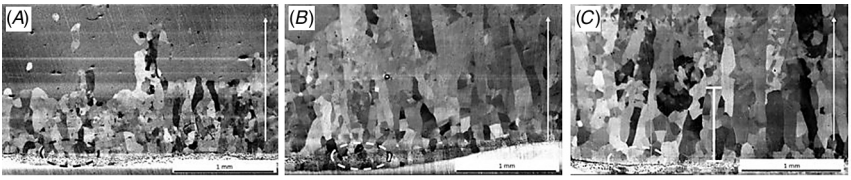

applied in the EBM process. A characteristic microstructure is shown for Specimen #1 (**fig. 5*A***). Niendorf et al.[8] already reported on AGG after solution annealing of SLM-processed Fe-Mn-Al-Ni. They assumed that residual stresses originating from the high-temperature gradients and rapid solidification in the SLM process (conducted at relatively low platform temperature) provided the necessary energy for some grains to grow abnormally.[33] However, the residual stresses in the EBM-processed Fe-Mn-Al-Ni should be comparatively low and, thus, it is more likely that the different microstructures in the as-built condition, being characterized by grain morphology and second phase distribution, affect AGG kinetics. It was shown that a change in the chemical composition (i.e., the addition of titanium and chromium to Fe-Mn-Al-Ni) has a significant effect on the morphology of the γ-phase of conventionally processed material, finally leading to pronounced changes in AGG kinetics and final grain sizes.[28] In-depth analysis of the AGG kinetics in AM Fe-Mn-Al-Ni after solution treatments is, however, beyond the scope of the present study and, thus, will be the subject of future work.

Besides random AGG in parts of the specimens, all sets of specimens reveal an area with a thickness of about 1 mm being characterized by a fundamentally different microstructural appearance. This is probably due to pronounced diffusion of chromium upon processing and during the annealing process. Furthermore, the segregations already mentioned in the case of the as-built condition grew during annealing. EDS analysis (not shown) demonstrated local enrichment in aluminum and nickel.

In order to investigate AGG promoted by cyclic heat treatment in AM-processed Fe-Mn-Al-Ni, specimens were subjected to the heat treatment procedure previously applied by Vollmer et al. (**fig. 1**).[28] Since Specimen #1 showed a too high density of defects, the procedure was only applied to Specimens #2 and #3. After cyclic heat treatment, Specimen #2 does not show pronounced grain coarsening,

FIG. 6 EBSD analysis (inverse pole figure maps) of (*A*) Parameter Set #2 and (*B*) Parameter Set #3 after the cyclic heat treatment and subsequent aging. Color coding is with respect to BD. Corresponding pole figures of the areas highlighted by the dashed boxes in (*A*) and (*B*) are shown in (*C*) and (*D*).

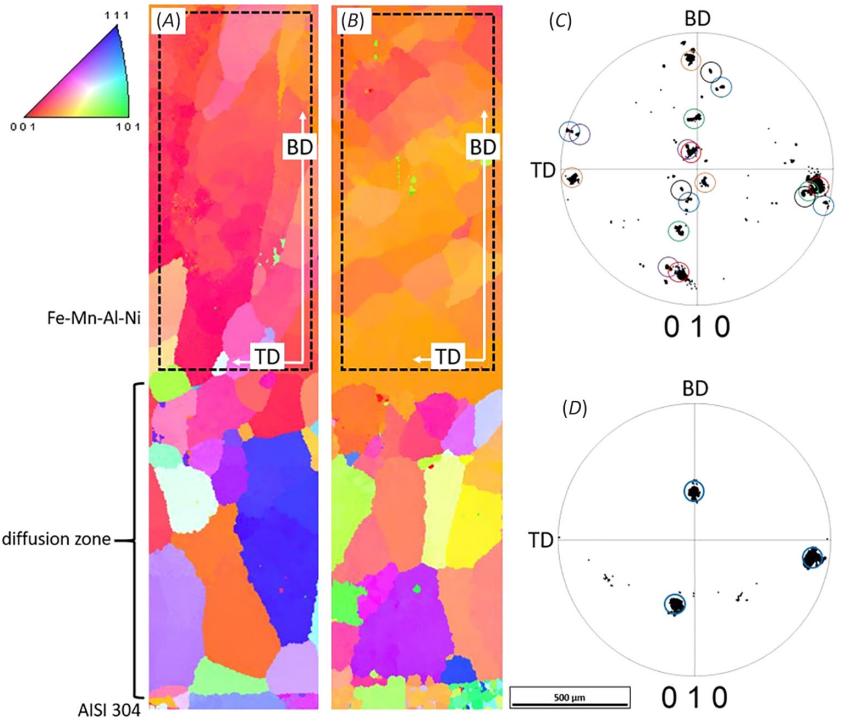

whereas in Specimen #3, a large-grained, assumedly single crystalline structure with a high density of subgrain structures was obtained, as can be deduced from the pole figures (**fig. 6*C*** and **6*D***) of the areas highlighted by the dashed boxes in **figure 6*A*** and **6*B***. Similar to the results after the solution annealing, AGG cannot be observed in all specimens after cyclic heat treatment. In Specimen #3, it is very likely that grain growth was already completed before the final solution annealing step because subgrain structures are only present in areas where the grain growth was already completed before the last solution annealing step.[28] The preferred orientation upon AGG (i.e., near ⟨001⟩) indicates that the EBM induced texture of the as-built condition can be maintained in the condition after AGG. However, a final evaluation of effects of initial texture on the grain orientation upon AGG here is difficult due to the limited number of specimens. Relationships will be further analyzed on a statistical basis in future work.

FIG. 7 SEM EDS mappings of the interface region (built plate below the superimposed red dashed line) for Parameter Set #3 after cyclic heat treatment.

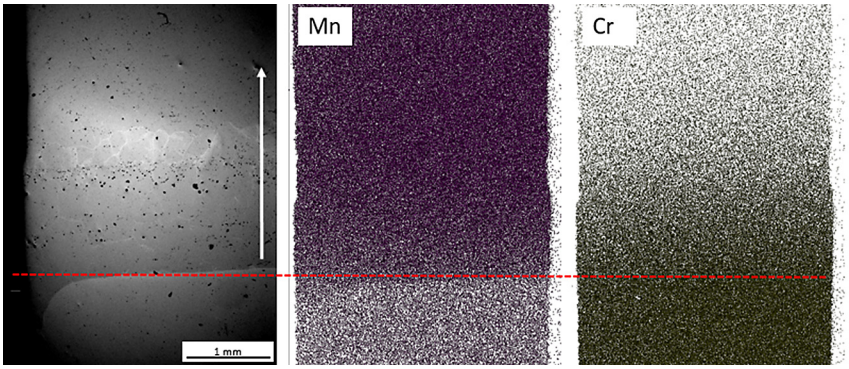

Again, a zone of about 1 mm, with a different microstructural appearance characterized by the absence of substantial grain growth, can be seen between the AISI 304 and the Fe-Mn-Al-Ni. The EDS mapping shown in **figure 7** clearly reveals that the zone, where grain growth is hampered, coincides with the diffusion zone of chromium. Recently, Vollmer et al.[28] revealed that the addition of chromium strongly inhibits AGG in Fe-Mn-Al-Ni. In light of these results, it is very likely that the growth of the single crystalline part stopped in specimen regions where a critical amount of chromium is exceeded.

INCREMENTAL STRAIN TEST

In order to study the overall performance of the AISI 304/Fe-Mn-Al-Ni compound, incremental strain tests (ISTs) were conducted on the specimen shown in **figure 6*B*** as well as on an AISI 304 reference specimen. The critical stress for plastic deformation of the latter is quite low (**fig. 8*A***), and it should be noted that the AISI 304 reference specimen reaches a stress of 400 MPa at approximately 8% applied strain. Taking into account that the share of AISI 304 is about half of the compound specimen and that no martensitic transformation has been observed in the very first cycles, it is obvious that, up to about 4% strain, the plastic deformation is mainly accommodated by the AISI 304, and the Fe-Mn-Al-Ni initially only deforms elastically. At about 4% applied strain, the stress level increased to about 400 MPa, and a martensitic transformation is seen for the first time in the Fe-Mn-Al-Ni alloy (not shown). This is in good agreement with results of Tseng et al.,[17] showing critical stresses of about 400 MPa for single-crystal Fe-Mn-Al-Ni with ⟨001⟩ orientation in compression after an aging treatment of 3 h at 200°C. In the course of further cycling, clear traces of pseudoelasticity can be seen. Fairly good reversibility of martensitic transformation can be deduced from the stress-strain curves indicated by the opening between the unloading and loading path.

In order to provide for deeper insights into the mechanical behavior, the stress-strain curve of the eighth cycle is highlighted in **figure 8*B***. It is obvious that the mechanical response is partially characterized by plastic deformation of the AISI 304 alloy; however, a significant contribution of the pseudoelastic deformation of the Fe-Mn-Al-Ni alloy can be seen as well. In situ micrographs of the loaded and unloaded condition obtained within the eighth cycle are shown in **figure 8*C*** and **8*D***, respectively. In the loaded condition (**figure 8*C***), pronounced topography changes, which can be linked to the deformation of the AISI 304, can be observed at the bottom of the micrograph. In contrast, martensitic structures can be seen in the Fe-Mn-Al-Ni single crystal in the upper part. These structures partly disappear upon unloading (**figure 8*D***), providing a proof of reversibility and, thus, pseudoelastic behavior. In addition, the grain boundaries within the diffusion zone are visible. It is assumed that the partly incomplete reversibility of the Fe-Mn-Al-Ni is linked to the interaction of the martensite with the subgrain structures,[28] martensite variant interaction,[16] as well as to effects related to the experimental setup (i.e., friction between the specimen and the grips). A certain amount of pores could also have a detrimental effect on the pseudoelastic behavior due to an interaction between

FIG. 8 Incremental strain test of an AISI 304 reference specimen and for an AISI 304/Fe-Mn-Al-Ni compound specimen (Parameter Set #3) after cyclic heat treatment. In (*A*), the responses recorded during the complete ISTs up to 12% are plotted; (*B*) detail highlighting only the eighth cycle of the AISI 304/Fe-Mn-Al-Ni compound specimen; (*C*) corresponding in situ OM images of the AISI 304/Fe-Mn-Al-Ni compound specimen in the loaded and (*D*) unloaded condition (see "x" in *B*).

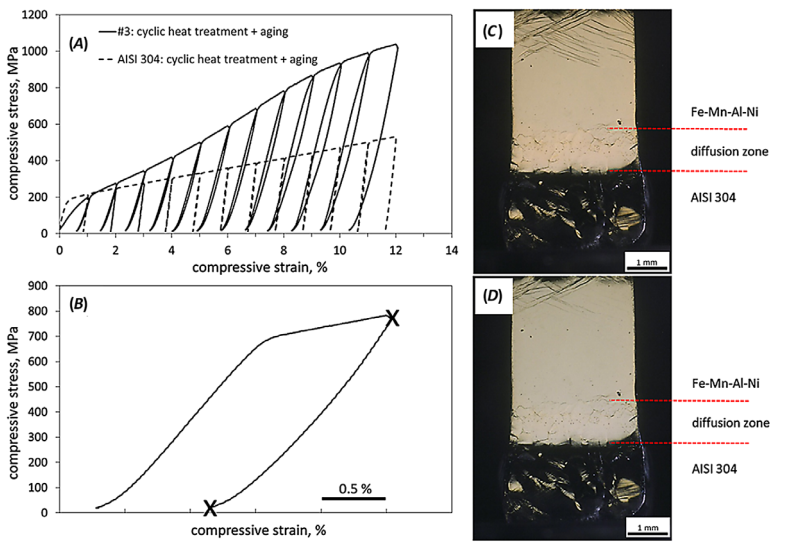

pores and martensite plates. Based on present results, quantitative analysis of the pseudoelastic performance is difficult. The plastic deformation of the AISI 304 can hardly be separated from the irrecoverable pseudoelastic strain of the Fe-Mn-Al-Ni. In-depth analysis of mechanical behavior using local strain evaluation by means of digital image correlation as well as an in-depth analysis of the microstructural features leading to the functional degradation will be the subject of follow-up studies.

Conclusions

The present study reveals the possibility of directly producing functionally graded Fe-Mn-Al-Ni/AISI 304 specimens with good pseudoelastic properties by using EBM. Due to the high process temperature and the lower cooling rates as compared to SLM, a crack-free microstructure was observed in the Fe-Mn-Al-Ni SMA. However, cracks occurred in the diffusion zone between the build plate and the SMA. This assumedly can be attributed to an insufficient amount of ductile γ phase at the grain boundaries in the deteriorated region, which is attributed to the diffusion of chromium from the substrate to the SMA. Subsequent heat treatments (i.e., solution annealing treatments and cyclic heat treatments) are adequate means to promote AGG in the Fe-Mn-Al-Ni alloy. Up to now, it remains an open question whether the strong texture after AM can be robustly maintained upon the AGG process. The in situ IST revealed a superimposed material response of the Fe-Mn-Al-Ni SMA and the austenitic stainless steel AISI 304. Primarily plastic deformation of the AISI 304 austenitic steel was observed at the beginning of the test followed by a partly reversible martensitic transformation of the SMA in later stages of the test. The polycrystalline diffusion zone of the Fe-Mn-Al-Ni showed hardly any martensitic transformation. To open up the full potential of multimaterial structures using Fe-Mn-Al-Ni as a functional alloy, future studies should focus on the application of high-strength structural materials.

ACKNOWLEDGMENTS

Financial support by Deutsche Forschungsgemeinschaft (Project No. 250216343; NI1327/7-3) within the Emmy Noether-Program is gratefully acknowledged.

References

1. J. T. Sehrt, S. Kleszczynski, and C. Notthoff, "Nanoparticle Improved Metal Materials for Additive Manufacturing," *Progress in Additive Manufacturing* 2 (2017): 179–191.
2. T. Niendorf, F. Brenne, P. Hoyer, D. Schwarze, M. Schaper, R. Grothe, M. Wiesener, G. Grundmeier, and H. J. Maier, "Processing of New Materials by Additive Manufacturing: Iron-Based Alloys Containing Silver for Biomedical Applications," *Metallurgical and Materials Transactions A* 46 (2015): 2829–2833.
3. T. Niendorf, F. Brenne, M. Schaper, A. Riemer, S. Leuders, W. Reimche, D. Schwarze, and H. J. Maier, "Labelling Additively Manufactured Parts by Microstructural Gradation—Advanced Copy-Proof Design," *Rapid Prototyping Journal* 22 (2016): 630–635.

4. H. Helmer, A. Bauereiß, R. F. Singer, and C. Körner, "Grain Structure Evolution in Inconel 718 during Selective Electron Beam Melting," *Materials Science and Engineering: A* 668 (2016): 180–187.
5. A. Hinojos, J. Mireles, A. Reichardt, P. Frigola, P. Hosemann, L. E. Murr, and R. B. Wicker, "Joining of Inconel 718 and 316 Stainless Steel Using Electron Beam Melting Additive Manufacturing Technology," *Materials & Design* 94 (2016): 17–27.
6. D. Deng, R. L. Peng, H. Söderberg, and J. Moverare, "On the Formation of Microstructural Gradients in a Nickel-Base Superalloy during Electron Beam Melting," *Materials & Design* 160 (2018): 251–261.
7. K. Otsuka and C. M. Wayman, *Shape Memory Materials* (Cambridge, UK: Cambridge University Press, 2002).
8. T. Niendorf, F. Brenne, P. Krooß, M. Vollmer, J. Günther, D. Schwarze, and H. Biermann, "Microstructural Evolution and Functional Properties of Fe-Mn-Al-Ni Shape Memory Alloy Processed by Selective Laser Melting," *Metallurgical and Materials Transactions A* 47 (2016): 2569–2573.
9. B. E. Franco, J. Ma, B. Loveall, G. A. Tapia, K. Karayagiz, J. Liu, A. Elwany, R. Arroyave, and I. Karaman, "A Sensory Material Approach for Reducing Variability in Additively Manufactured Metal Parts," *Scientific Reports* 7 (2017): 3604.
10. J. Ma, B. Franco, G. Tapia, K. Karayagiz, L. Johnson, J. Liu, R. Arroyave, I. Karaman, and A. Elwany, "Spatial Control of Functional Response in 4D-Printed Active Metallic Structures," *Scientific Reports* 7 (2017): 46707.
11. Q. Zhou, M. D. Hayat, G. Chen, S. Cai, X. Qu, H. Tang, and P. Cao, "Selective Electron Beam Melting of NiTi: Microstructure, Phase Transformation and Mechanical Properties," *Materials Science and Engineering: A* 744 (2019): 290–298.
12. T. Omori, K. Ando, M. Okano, X. Xu, Y. Tanaka, I. Ohnuma, R. Kainuma, and K. Ishida, "Superelastic Effect in Polycrystalline Ferrous Alloys," *Science* 333, no. 6038 (2011): 68–71.
13. L. W. Tseng, J. Ma, S. J. Wang, I. Karaman, M. Kaya, Z. P. Luo, and Y. I. Chumlyakov, "Superelastic Response of a Single Crystalline FeMnAlNi Shape Memory Alloy under Tension and Compression," *Acta Materialia* 89 (2015): 374–383.
14. L. W. Tseng, J. Ma, S. J. Wang, I. Karaman, and Y. I. Chumlyakov, "Effects of Crystallographic Orientation on the Superelastic Response of FeMnAlNi Single Crystals," *Scripta Materialia* 116 (2016): 147–151.
15. M. Vollmer, M. J. Kriegel, A. Walnsch, V. Klemm, A. Leineweber, and T. Niendorf, "On the Microstructural and Functional Stability of Fe-Mn-Al-Ni at Ambient and Elevated Temperatures," *Scripta Materialia* 162 (2019): 442–446.
16. M. Vollmer, M. J. Kriegel, P. Krooß, S. Martin, V. Klemm, A. Weidner, Y. Chumlyakov, H. Biermann, D. Rafaja, and T. Niendorf, "Cyclic Degradation Behavior of ⟨001⟩-Oriented Fe–Mn–Al–Ni Single Crystals in Tension," *Shape Memory and Superelasticity* 4 (2017) 335–346.
17. L. W. Tseng, J. Ma, B. C. Hornbuckle, I. Karaman, G. B. Thompson, Z. P. Luo, and Y. I. Chumlyakov, "The Effect of Precipitates on the Superelastic Response of [1 0 0] Oriented FeMnAlNi Single Crystals under Compression," *Acta Materialia* 97 (2015): 234–244.
18. L. W. Tseng, J. Ma, Y. I. Chumlyakov, and I. Karaman, "Orientation Dependence of Superelasticity in FeMnAlNi Single Crystals under Compression," *Scripta Materialia* 166 (2019): 48–52.
19. L. W. Tseng, J. Ma, M. Vollmer, P. Krooß, T. Niendorf, and I. Karaman, "Effect of Grain Size on the Superelastic Response of a FeMnAlNi Polycrystalline Shape Memory Alloy," *Scripta Materialia* 125 (2016): 68–72.

20. H. Ozcan, J. Ma, S. J. Wang, I. Karaman, Y. Chumlyakov, J. Brown, and R. D. Noebe, "Effects of Cyclic Heat Treatment and Aging on Superelasticity in Oligocrystalline Fe-Mn-Al-Ni Shape Memory Alloy Wires, *Scripta Materialia* 134 (2017): 66–70.
21. H. Ozcan, J. Ma, I. Karaman, Y. I. Chumlyakov, R. Santamarta, J. Brown, and R. D. Noebe, "Microstructural Design Considerations in Fe-Mn-Al-Ni Shape Memory Alloy Wires: Effects of Natural Aging," *Scripta Materialia* 142 (2018): 153–157.
22. T. Omori, M. Okano, and R. Kainuma, "Effect of Grain Size on Superelasticity in Fe-Mn-Al-Ni Shape Memory Alloy Wire," *APL Materials* 1 (2013): 32103.
23. M. Vollmer, C. Segel, P. Krooß, J. Günther, L. W. Tseng, I. Karaman, A. Weidner, H. Biermann, and T. Niendorf, "On the Effect of Gamma Phase Formation on the Pseudoelastic Performance of Polycrystalline Fe–Mn–Al–Ni Shape Memory Alloys," *Scripta Materialia* 108 (2015): 23–26.
24. M. Vollmer, P. Krooß, M. J. Kriegel, V. Klemm, C. Somsen, H. Ozcan, I. Karaman, A. Weidner, D. Rafaja, H. Biermann, and T. Niendorf, "Cyclic Degradation in Bamboo-Like Fe–Mn–Al–Ni Shape Memory Alloys—The Role of Grain Orientation," *Scripta Materialia* 114 (2016): 156–160.
25. T. Omori, T. Kusama, S. Kawata, I. Ohnuma, Y. Sutou, Y. Araki, K. Ishida, and R. Kainuma, "Abnormal Grain Growth Induced by Cyclic Heat Treatment," *Science* 341 (2013): 1500–1502.
26. T. Omori, H. Iwaizako, and R. Kainuma, "Abnormal Grain Growth Induced by Cyclic Heat Treatment in Fe-Mn-Al-Ni Superelastic Alloy," *Materials & Design* 101 (2016): 263–269.
27. T. Kusama, T. Omori, T. Saito, S. Kise, T. Tanaka, Y. Araki, and R. Kainuma, "Ultra-Large Single Crystals by Abnormal Grain Growth," *Nature Communications* 8 (2017): 354.
28. M. Vollmer, T. Arold, M. J. Kriegel, V. Klemm, S. Degener, J. Freudenberger, and T. Niendorf, "Promoting Abnormal Grain Growth in Fe-Based Shape Memory Alloys through Compositional Adjustments," *Nature Communications* 10 (2019): 2337.
29. S. Tammas-Williams, H. Zhao, F. Léonard, F. Derguti, I. Todd, and P. B. Prangnell, "XCT Analysis of the Influence of Melt Strategies on Defect Population in Ti–6Al–4V Components Manufactured by Selective Electron Beam Melting," *Materials Characterization* 102 (2015): 47–61.
30. W. Kurz, C. Bezençon, and M. Gäumann, "Columnar to Equiaxed Transition in Solidification Processing," *Science and Technology of Advanced Materials* 2 (2001): 185–191.
31. M. Vollmer, P. Krooß, I. Karaman, and T. Niendorf, "On the Effect of Titanium on Quenching Sensitivity and Pseudoelastic Response in Fe-Mn-Al-Ni-Base Shape Memory Alloy," *Scripta Materialia* 126 (2017): 20–23.
32. J. Günther, F. Brenne, M. Droste, M. Wendler, O. Volkova, H. Biermann, and T. Niendorf, "Design of Novel Materials for Additive Manufacturing—Isotropic Microstructure and High Defect Tolerance," *Scientific Reports* 8 (2018): 1298.
33. L. Thijs, F. Verhaeghe, T. Craeghs, J. van Humbeeck, and J.-P. Kruth, "A Study of the Microstructural Evolution during Selective Laser Melting of Ti–6Al–4V," *Acta Materialia* 58 (2010): 3303–3312.